

Black hole X-ray binary A0620–00 in quiescence: hints of Faraday rotation of near-infrared and optical polarization?

Vadim Kravtsov¹, Alexandra Veledina^{1,2}, Andrei V. Berdyugin¹, Sergey Tsygankov¹, Tariq Shahbaz^{3,4}, Manuel A. P. Torres^{3,4}, Helen Jermak⁵, Callum McCall⁵, Jari J. E. Kajava^{1,6}, Vilppu Piirola¹, Takeshi Sakano⁷, Masato Kagitani⁷, Svetlana V. Berdyugina^{8,9}, and Juri Poutanen¹

¹ Department of Physics and Astronomy, FI-20014 University of Turku, Finland
e-mail: vakrau@utu.fi

² Nordita, KTH Royal Institute of Technology and Stockholm University, Hannes Alfvéns väg 12, SE-10691 Stockholm, Sweden

³ Instituto de Astrofísica de Canarias, E-38205 La Laguna, Tenerife, Spain

⁴ Departamento de Astrofísica, Universidad de La Laguna, E-38206 La Laguna, Tenerife, Spain

⁵ Astrophysics Research Institute, Liverpool John Moores University, 146 Brownlow Hill, Liverpool L3 5RF, United Kingdom

⁶ Serco for the European Space Agency (ESA), European Space Astronomy Centre, Camino Bajo del Castillo s/n, E-28692 Villanueva de la Cañada, Madrid, Spain

⁷ Graduate School of Sciences, Tohoku University, Aoba-ku, 980-8578 Sendai, Japan

⁸ Istituto Ricerche Solari Aldo e Cele Daccò (IRSOL), Faculty of Informatics, Università della Svizzera italiana, 6605 Locarno, Switzerland

⁹ Institut für Sonnenphysik (KIS), Georges-Köhler-Allee 401a, 79110 Freiburg, Germany

July 11, 2024

ABSTRACT

We present simultaneous high-precision optical polarimetric and near-infrared (NIR) to ultraviolet (UV) photometric observations of low-mass black hole X-ray binary A0620–00 in the quiescent state. Subtracting interstellar polarization, estimated from a sample of field stars, we derive the intrinsic polarization of A0620–00. We show that the intrinsic polarization degree (PD) is variable with the orbital period with the amplitude of $\sim 0.3\%$ at least in the R band, where the signal-to-noise ratio of our observations is the best. It implies that some fraction of the optical polarization is produced by scattering of stellar radiation off the matter that follows the black hole in its orbital motion. In addition, we see a rotation of the orbit-average intrinsic polarization angle (PA) with the wavelength from 164° in the R to 180° in the B band. All of the above, combined with the historical NIR to optical polarimetric observations, shows the complex behavior of average intrinsic polarization of A0620–00 with the PA making continuous rotation from infrared to blue band by $\sim 56^\circ$ in total, while the PD $\sim 1\%$ remains nearly constant over the entire spectral range. The spectral dependence of the PA can be described by Faraday rotation with the rotation measure of $RM = -0.2 \text{ rad } \mu\text{m}^{-2}$, implying a few Gauss magnetic field in the plasma surrounding the black hole accretion disk. However, our preferred interpretation for the peculiar wavelength dependence is the interplay between two polarized components with different PAs. Polarimetric measurements in the UV range can help distinguishing between these scenarios.

Key words. accretion, accretion disks – polarization – stars: black holes – stars: individual: A0620–00 – X-rays: binaries

1. Introduction

A0620–00 is the prototypical low-mass X-ray binary (LMXB) system containing a black hole (BH), discovered during its 1975 outburst (Elvis et al. 1975). Its luminosity increased by more than a million times compared to the quiescent levels reaching the Eddington luminosity. Since then, the object has resided in the quiescent state, where its spectrum is dominated by the emission of $0.4M_\odot$ K-type star orbiting a $\sim 6M_\odot$ BH (McClintock & Remillard 1986; van Grunsven et al. 2017) with the period of $P_{\text{orb}} = 7.75$ h. Nevertheless, an additional source of non-stellar origin is needed to describe the excess of radio, near-infrared (NIR), and ultraviolet (UV) emission of A0620–00 near quiescence (McClintock et al. 1995; Froning et al. 2011; Gallo et al. 2019; Cherepashchuk et al. 2019). There is still no agreement on the nature of the additional component: it could be the jet, the accretion disk, the inner accretion flow, the gas stream, or some combination of the above. Different components may give similar contributions to the final spectrum, therefore additional

information is needed to distinguish between them. Polarization of the optical radiation may provide such information.

Indeed, optical and NIR radiation produced in various physical processes, including electron scattering of stellar radiation off the accretion disk/flow and synchrotron emission in the presence of the ordered magnetic field, can be polarized. The polarization degree (PD), polarization angle (PA), and their spectral properties are different for different processes, which makes polarimetry a powerful technique for studies of the physical mechanisms responsible for the optical and NIR emission production in BH X-ray binaries. A recent systematic study has shown, however, that in many quiescent BHs, the intrinsic optical polarization (corrected for interstellar contribution) is very small – in most cases $P_{\text{int}} \lesssim 0.5\%$ (Kravtsov et al. 2022). On the other hand, several LMXBs show significant polarization during (or near) the quiescence: MAXI J1820+070 demonstrated high (up to 5%) PD with the blue spectrum and PA different from the jet direction, suggesting BH spin-orbit misalignment (Poutanen et al. 2022);

Table 1. Log of polarimetric and photometric observations of A0620–00 in December 2022.

Telescope	UT Date 2022	Filters	N_{obs}
NOT	Dec 24–26	B, V, R	2
GTC	Dec 25	K_s, H, J	1
LT	Dec 20–24	u, g, r, i, z, B, V	3
UVOT	Dec 23–26	$B, V, u, w1, m2, w2$	4

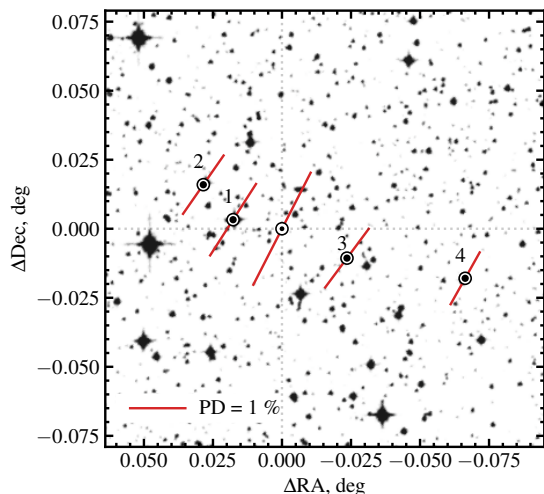


Fig. 1. Polarization map for A0620–00 (at the origin) and field stars in R band. The lines correspond to the observed polarization with the length of the bars showing the PD, and the direction indicating the PA (measured from north to east).

A0620–00 showed $\sim 1\%$ optical and NIR polarization in the quiescent state (Dubus et al. 2008; Russell et al. 2016).

Residing in the X-ray quiescence, A0620–00 shows optical state changes: according to the Cantrell et al. (2008) classification, there are two different states of the optical activity — passive and active. In the passive state, variations of the optical flux are consistent with the ellipsoidal variations, produced by the rotation of the tidally distorted optical companion. In the active state, the source is 20% brighter and shows an aperiodic high-frequency variation usually called “flickering”.

In this paper, we present the results of quasi-simultaneous high-precision optical polarimetric and multiwavelength (NIR to UV) photometric observations of A0620–00 during its passive quiescent state. The paper is organized as follows. In Sect. 2, we describe the observational data. In Sect. 3, we present the main results of our study: determination of the intrinsic optical polarization of A0620–00, its significant orbital variability, and rotation of the average intrinsic polarization angle with wavelength. In Sect. 4, we discuss possible physical mechanisms that can reproduce the observed behavior. Finally, in Sect. 5 we summarize our findings.

2. Data acquisition and analysis

2.1. Optical polarimetric observations

High-precision optical polarimetric observations of A0620–00 were performed using broad-band BVR polarimeter DIPol-UF (Pirola et al. 2021), a visitor instrument installed at the 2.56 m

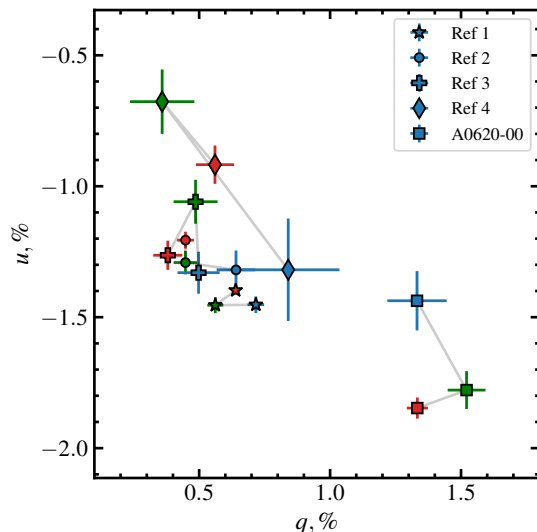


Fig. 2. Observed orbit-averaged Stokes parameters of A0620–00 (squares) and field stars in the $B, V,$ and R bands (blue, green, and red markers, respectively).

Nordic Optical Telescope (NOT), Observatorio del Roque de los Muchachos, La Palma, Spain. Field stars used for the interstellar polarization estimation were observed with DIPol-2 (Pirola et al. 2014), mounted on the remotely-controlled 60 cm Tohoku telescope (T60) at Haleakala Observatory, Hawaii. Both polarimeters utilize a “double-image” design that effectively eliminates the polarization of the sky, even if it varies throughout the observations. The instrumental polarization is small ($< 10^{-4}$) and well-calibrated by observing 20 unpolarized standard stars. The zero points of the PAs were determined by observing highly polarized standards HD 236928 and HD 25443. A more detailed description of the methods and calibrations can be found in Pirola et al. (2020) and Kravtsov et al. (2022), and references therein.

A0620–00 was observed during two nights between 2022 December 24–26 and 140 and 52 individual measurements of the Stokes parameters were made during the two nights, respectively. The first observation was continuous, 8 h long, and hence covered the whole orbital period of the binary, while the second observation covered only 40% of the period. Hereafter we will refer to the average polarization measured during the first observation as orbit-averaged polarization. Each individual linear polarization measurement was obtained from four consecutive images with 50-s exposures taken at different half-wave plate positions, resulting in one polarization measurement per ~ 3.3 min. To increase the signal-to-noise ratio, we split the data into bins so that each bin contains 10 individual measurements of the Stokes parameters. The errors of the normalized Stokes parameters q and u were computed as the standard errors of the weighted mean values within the bin. The Stokes parameters (q, u) then were translated into the PD P and PA θ ,

$$P = \sqrt{q^2 + u^2}, \quad \theta = \frac{1}{2} \text{atan2}(u, q). \quad (1)$$

The uncertainty on the PD is equal to the uncertainty of the individual Stokes parameters, and uncertainty on the PA in radians was estimated as $\sigma_\theta = \sigma_P / (2P)$ (Serkowski 1962; Kosenkov et al. 2017).

Table 2. Polarization of field stars.

Field star	Parallax (mas)	<i>B</i>		<i>V</i>		<i>R</i>	
		<i>q</i> (%)	<i>u</i> (%)	<i>q</i> (%)	<i>u</i> (%)	<i>q</i> (%)	<i>u</i> (%)
Ref 1	0.72 ± 0.04	0.71 ± 0.03	−1.45 ± 0.03	0.56 ± 0.03	−1.45 ± 0.03	0.64 ± 0.02	−1.40 ± 0.02
Ref 2	0.87 ± 0.02	0.64 ± 0.07	−1.32 ± 0.07	0.45 ± 0.04	−1.29 ± 0.04	0.45 ± 0.03	−1.20 ± 0.03
Ref 3	0.56 ± 0.02	0.50 ± 0.08	−1.33 ± 0.08	0.49 ± 0.08	−1.06 ± 0.08	0.38 ± 0.06	−1.26 ± 0.06
Ref 4	0.55 ± 0.02	0.84 ± 0.20	−1.32 ± 0.20	0.36 ± 0.12	−0.68 ± 0.12	0.56 ± 0.07	−0.92 ± 0.07

Table 3. One-orbit-average observed and intrinsic PD and PA of A0620–00 together with interstellar polarization estimate.

Filter	Observed		Interstellar		Intrinsic	
	P_{obs} (%)	θ_{obs} (deg)	P_{is} (%)	θ_{is} (deg)	P_{int} (%)	θ_{int} (deg)
<i>B</i>	1.96 ± 0.11	156 ± 2	1.61 ± 0.03	148 ± 1	0.62 ± 0.11	180 ± 5
<i>V</i>	2.34 ± 0.07	155 ± 1	1.56 ± 0.03	146 ± 1	1.01 ± 0.07	170 ± 2
<i>R</i>	2.27 ± 0.04	153 ± 1	1.54 ± 0.02	147 ± 1	0.83 ± 0.04	164 ± 2

2.2. Multiwavelength photometry

Quasi-simultaneous multiwavelength photometric observational campaign was organized on several telescopes (see Table 1). Near-infrared *JHK* photometry was made using EMIR wide-field imager (Garzón et al. 2022), installed on the 10.4 m Gran Telescopio Canarias (GTC), La Palma, Spain. Observations in the broadband SDSS-*ugriz*, Bessel *V*, and Bessel *B* filters were performed using IO:O instrument of the 2-m Liverpool Telescope (LT; Steele et al. 2004), La Palma, Spain. For all the instruments, basic data reductions such as bias and dark subtraction and flat fielding are done via the internal common pipelines.

2.3. Swift/UVOT

The Neil Gehrels Swift Observatory (Gehrels et al. 2004) observed A0620–00 four times from 2022 December 23 to 26 (see Table 1) with total exposure of about 7 ks. The image analysis has been done following the procedure provided by the UK Swift Science Data Centre.¹ Photometry in all available filters (*V*, *B*, *U*, *UVW1*, *UVW2*, and *UVM2*) was performed using the tool UVOTSOURCE from the HEASOFT package version 6.32 and the latest calibration files. The source and background photons were extracted from the apertures with radii of 5'' and 10'', respectively. The background was chosen with the center about 18'' away from the source for all filters.

For the spectral fitting, all available data were converted to the spectral files. For the Swift/UVOT data the UVOT2PHA tool was applied using the corresponding response files in the CALDB. All other data were converted to the spectral files using tool FTFLX2XSP from the FTOOLS package. The following spectral fitting was performed using XSPEC version 12.13.1 (Arnaud 1996).

3. Results

3.1. Average intrinsic polarization

The observed optical polarization of a distant star is a combination of the intrinsic polarization of the object and interstellar (IS) polarization. The main source of the interstellar polarization (q_{is} , u_{is}) is the optical dichroism of non-spherical interstellar dust particles aligned by Galactic magnetic field. To extract the intrinsic polarization (q_{int} , u_{int}) of A0620–00 from the observed polarization (q_{obs} , u_{obs}), we first estimated the IS polarization. We measured the polarization of the four close field stars (see Fig. 1

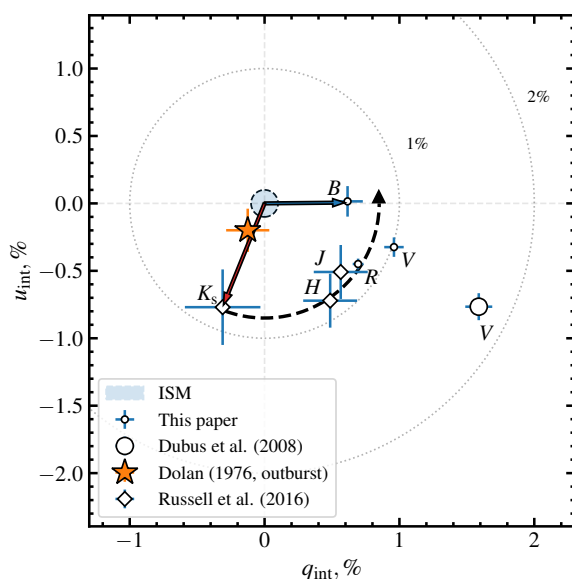


Fig. 3. Intrinsic Stokes parameters of the polarization of A0620–00 in quiescence measured in different filters from the K_s to B as indicated by letters near each data point. The light blue circle at the origin illustrates the uncertainty of the interstellar polarization. The red and blue arrows indicate the intrinsic polarization vector directions in K_s and B bands, respectively. The dashed curved arrow shows the track left by the intrinsic polarization vector during its rotation from the IR to the blue part of the spectrum. An orange star shows the polarization of A0620–00 measured during the 1975 outburst by Dolan (1976).

and Tab. 2) with similar parallaxes according to Gaia DR3 (Gaia Collaboration et al. 2021) and, taking into account the proximity of the star both in parallax and in angular distance on the image, we choose the polarization of the star Ref 1 as the best IS polarization estimate in the direction of A0620–00. Our estimate of the IS polarization of $P \sim 1.5\%$ and $\theta \sim 147^\circ$ (see Table 3) is consistent with the previous estimates in the *V* band of $P \sim 1.5\%$ and $\theta \sim 153^\circ$ by Dubus et al. (2008) and $P \sim 1.7\%$ and $\theta \sim 142^\circ$ by Dolan (1976).

Subtracting the interstellar component from the observed polarization, we find the average intrinsic polarization of A0620–00 to be $P = 0.6\text{--}1.0\%$ with θ changing from 164° in the *R* filter to 180° in *B* (see Table 3). Combining NIR polarimetric observations (Russell et al. 2016) corrected for IS polarization with our optical measurements, we see the continuous rotation of

¹ <https://www.swift.ac.uk/analysis/uvot/>

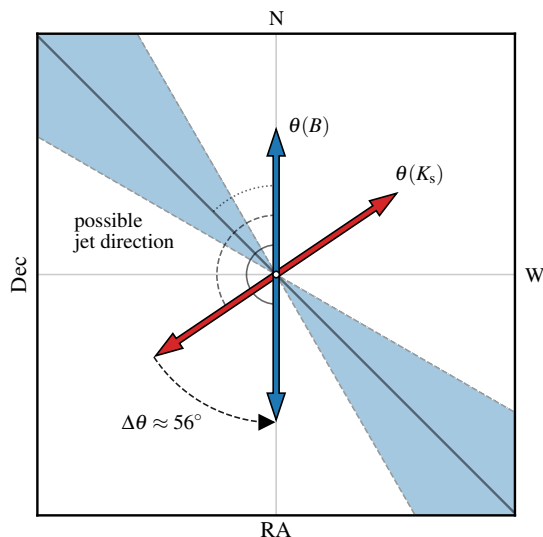


Fig. 4. Rotation of the polarization on the sky. Red and blue arrows correspond to the direction of the polarization in the B and K_s filters, respectively. The blue region shows the direction of the radio ejections as measured in [Kuulkers et al. \(1999\)](#).

the intrinsic polarization vector with the wavelength from NIR to B (see Fig. 3). The amplitude of the polarization vector rotation on the sky is $\Delta\theta = \theta(B) - \theta(K_s) \approx 56^\circ$ (see Fig. 4). In contrast to the PA, PD barely changes with wavelength remaining at $\sim 1\%$ level from K_s to B band.

We note that although the determination of the intrinsic PA strongly depends on the accuracy of the IS polarization estimate, there are several additional reasons to believe that the intrinsic polarization estimate is close to its true value. First of all, our estimation of the IS polarization is consistent with the previous independent measurements ([Dubus et al. 2008](#); [Dolan 1976](#)). Furthermore, although the observed PD of A0620–00 in [Dubus et al. \(2008\)](#) V -band observations was significantly higher than in this paper, subtracting our estimate of the IS polarization from their observed Stokes parameters, we get the PA of intrinsic polarization matching our value within a few degrees – this can be seen in Fig. 3, if one connects the origin to the corresponding observational points and compare the directions of the resulting vectors. This alignment of the intrinsic polarization vectors is unlikely to be coincidental and confirms our IS polarization estimate.

3.2. Orbital variability of the polarization

We folded the photometric and polarimetric observations of A0620–00 in R -band (for which the S/N is the best) with the orbital period using the recent ephemeris of [Cherepashchuk et al. \(2019\)](#). We find statistically significant orbital variability of intrinsic polarization of the source in the R filter (Fig. 5b,c). We plot the orbital profile of the observed polarization together with the optical light curve of A0620–00, obtained simultaneously (Fig. 5a). We see that the polarization degree is constant within the measurement errors during the first half of the orbit, and varies significantly in the second half. Variations of PD follow closely the variations of the R -band magnitudes. The absence of flickering in the photometric observations together with the visual magnitude $V = 18.3 \pm 0.1$ of A0620–00 suggests that the

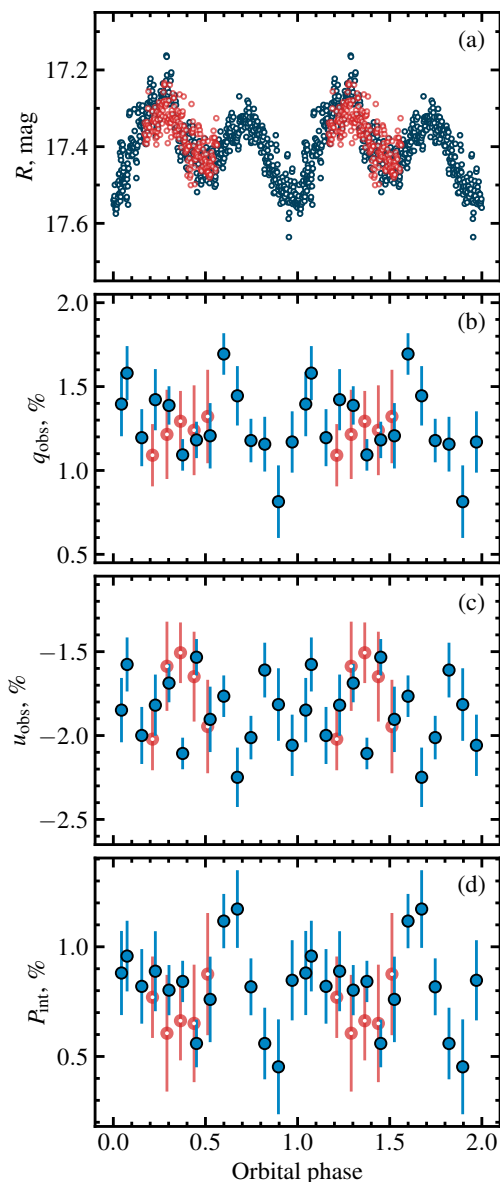


Fig. 5. Orbital profiles of the flux and of the normalized Stokes parameters of A0620–00. Blue solid and red empty circles correspond to the data from two different orbits. *Panel (a)*: photometric R magnitudes of A0620–00 folded with the orbital period. *Panels (b) and (c)*: observed normalized Stokes parameters. *Panel (d)*: intrinsic PD of A0620–00 in the R filter folded with the orbital period. Each circle with the 1σ error bar shows the 35-min average polarization.

source was in the passive quiescent state during our campaign ([Cantrell et al. 2008](#)).

3.3. Broadband spectrum

The observed NIR-to-UV spectral energy distribution (SED) of A0620–00 corrected for reddening assuming $E(B - V) = 0.35$ ([Wu et al. 1983](#)) is shown in Fig. 6. The key feature of the SED is the excess of UV photons, previously observed in the quiescent state ([Froning et al. 2011](#); [McClintock et al. 1995](#)) – an extra source of UV radiation in addition to the optical companion is needed to reproduce the observed shape of the spectrum. The spectrum alone, however, does not allow unambiguous sep-

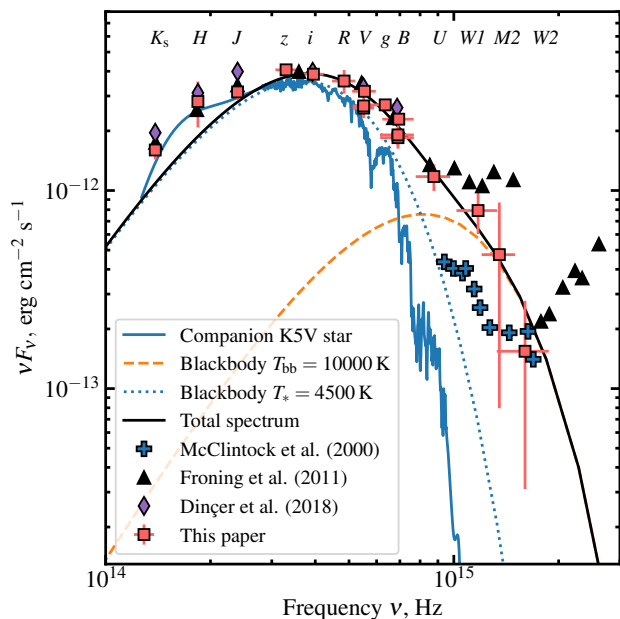


Fig. 6. Spectral energy distribution of A0620–00, corrected for reddening assuming $E(B - V) = 0.35$. Red squares with error bars correspond to the data from this paper. Blue crosses, black triangles and purple diamonds show data from McClintock & Remillard (2000), Froning et al. (2011), and Dinçer et al. (2018), respectively. Solid blue, dotted blue, and dashed orange lines show the spectra of the K5V star (Pickles 1998), the blackbody of $T_* = 4500$ K and an additional blackbody of $T_{bb} = 10,000$ K, respectively.

aration of the second component: even the simplest model with one additional blackbody is degenerate due to the uncertainty in the stellar spectrum normalization. Various different methods were used to estimate the contribution of non-stellar emission to the quiescent spectrum of A0620–00 (Marsh et al. 1994; Gelino et al. 2001; Harrison et al. 2007; Froning et al. 2011; Dinçer et al. 2018). Despite the fact that there is no complete consensus, it can be cautiously noted that most authors agree that the companion star dominates the entire NIR-to-optical range, with the contribution of additional component increasing towards the blue part of the spectrum. The additional component becomes comparable with the stellar flux only near B band, where its contribution reaches 20–50%. Non-stellar emission spectrum can be described with the blackbody of temperature $T_{bb} = 9,000$ – $11,000$ K depending on the state of activity. The nature of the additional component is still under discussion, but most likely it corresponds to the brightest part of the accretion disk (either to the hot inner disk regions or to the bright spot formed at the impact point of the accretion stream). The bright spot is clearly present in the Doppler tomograms (Marsh et al. 1994; Shahbaz et al. 1994, 2004; Neilsen et al. 2008) and it is needed to explain the asymmetric light curves (Froning & Robinson 2001; Cantrell et al. 2010; van Grunsven et al. 2017; Cherepashchuk et al. 2019). The contribution of the non-stellar radiation is variable on short (Haswell et al. 1993) and long (Cantrell et al. 2008) timescales. Our new observations are consistent with both interpretations (see Fig. 6 and Sect. 4).

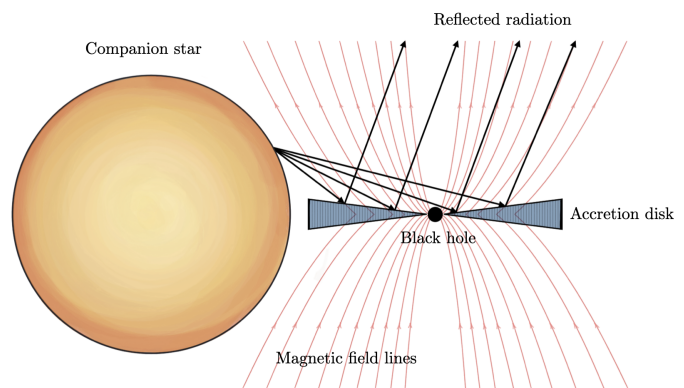


Fig. 7. Schematic illustration of the scattering geometry (not to scale).

4. Discussion

4.1. The source of the polarization

The polarization measurements of optical light from the binary were obtained both in the quiescent state and in the outburst (Dolan 1976, see the orange star in Fig. 3). The observed PD, PA, and their spectral properties were found to be consistent with the interstellar origin. Our IS polarization estimate is very close to the outburst polarization level of A0620–00, which confirms the above statement. Sub-per cent intrinsic optical polarization of A0620–00 is in line with that of the other X-ray binaries – most known sources observed during the outburst show low intrinsic polarization levels (XTE J1118+480, Schultz et al. 2004; MAXI J0637–430, Kravtsov et al. 2019; MAXI J1820+070, Veledina et al. 2019; Kosenkov et al. 2020; SwiftJ 1727.8–1613, Kravtsov et al. 2023a). However, some BH LMXBs show a significant increase of intrinsic PD as they approach quiescence (e.g., MAXI J1820+070, Poutanen et al. 2022, and A0620–00, Dubus et al. 2008).

The orbit-averaged intrinsic polarization of A0620–00 in the quiescent state has nearly the same PD $\sim 1\%$ at all wavelengths from K_s to B band, yet PA shows a significant rotation over those wavelengths (Fig. 3). This makes A0620–00 the only source known to date for which such a strong PA dependence on the wavelength is observed. Such polarization behavior cannot be explained in terms of simple mechanisms of polarization production. Indeed, if the polarization is produced mostly by scattering, its PA should not depend on the wavelength.

We first study the case where Faraday rotation causes the observed dependence of PA on wavelength. We consider the scenario illustrated in Fig. 7. The unpolarized radiation of the companion star gets scattered by the accretion disk and the polarized scattered radiation has initial PA independent of the wavelength. After the scattering, the linearly polarized radiation propagates toward the observer through the magnetized plasma surrounding the accretion disk. The PA of the light propagating along the magnetic field lines experiences the Faraday rotation, resulting in the observed PA dependence on wavelength.

The PA of linearly polarized radiation propagating through the magnetized plasma rotates with the wavelength λ as:

$$\theta(\lambda) = \theta_0 + \text{RM} \lambda^2, \quad (2)$$

where the rotation measure RM is defined through the integral along the line of sight

$$\text{RM} = \frac{e^3}{2\pi m_e^2 c^4} \int n_e(l) B_{\parallel}(l) dl, \quad (3)$$

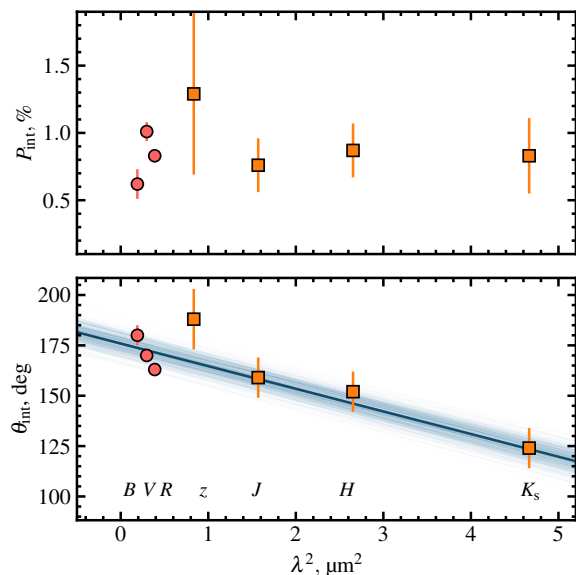


Fig. 8. Dependence of the intrinsic PD and PA of A0620–00 on λ^2 . The circles and squares correspond to optical observations from this paper and NIR polarimetric observations from Russell et al. (2016), respectively. The blue line shows the best-fit Faraday rotation model given by Eq. (2).

where n_e is the electron number density, B_{\parallel} (in G) is the line of sight magnetic field strength, e is the electric charge, m_e is the electron mass and c is the speed of light. If B_{\parallel} is constant, the RM can be expressed through the Thomson optical depth $\tau_T = \int n_e \sigma_T dl$. In this case, $RM \approx 0.4 \tau_T B_{\parallel} \text{ rad } \mu\text{m}^{-2}$.

We use Eq. (2) with parameters θ_0 and RM to find the best-fit solution for the Faraday rotation of PA in our optical points and NIR points reported in Russell et al. (2016). We find the best-fit parameters $\theta_0 = 175^\circ \pm 4^\circ$ and $RM = -0.20 \pm 0.01 \text{ rad } \mu\text{m}^{-2}$ (see Fig. 8). The latter value gives the relation between the line-of-sight optical depth and magnetic field (in Gauss) $\tau_T B_{\parallel} \approx 0.5$. For the realistic values of matter density in quiescence $\tau_T \lesssim 0.1$, we find $B \gtrsim 5$ G. The latter value is roughly consistent with the magnetic fields expected in the quiescent-state optically thin accretion flows (Wallace & Pe’er 2021), which may be similar to those of optically thin plasma surrounding the disk (Fig. 7).

We note, however, that the NIR data have been taken almost ten years prior to our optical observations, hence potential magnetic field variations may lead to the inconsistency of trends between the optical and NIR PA points. We indeed observe that our recent measurements (leftmost three points in Fig. 8) lie on a straight line with the slope differing from the general trend. If we apply Eq (2) only to our data, we obtain $\theta_0 = 186^\circ \pm 6^\circ$ and $RM = -1.3 \pm 0.3 \text{ rad } \mu\text{m}^{-2}$ (see Fig. 8). This translates to $\tau_T B_{\parallel} \approx 3.2$, requiring almost seven times higher magnetic field strength for the Faraday rotation to occur in the optically thin plasma ($\tau_T \lesssim 1$). We also note that the Thomson scattering and Faraday effect cannot explain the complex dependence of PD on energy, with P_V being higher than P_R and P_B . The sharp rise of polarization in a narrow wavelength range may be related to the atomic features.

Next, we consider the scenario where the observed polarization arises from two components: one coming from the scattering of the stellar light and the other from the polarized contribution of the additional UV component. Stellar polarization is assumed to have constant PD and PA which implies a constant fraction of

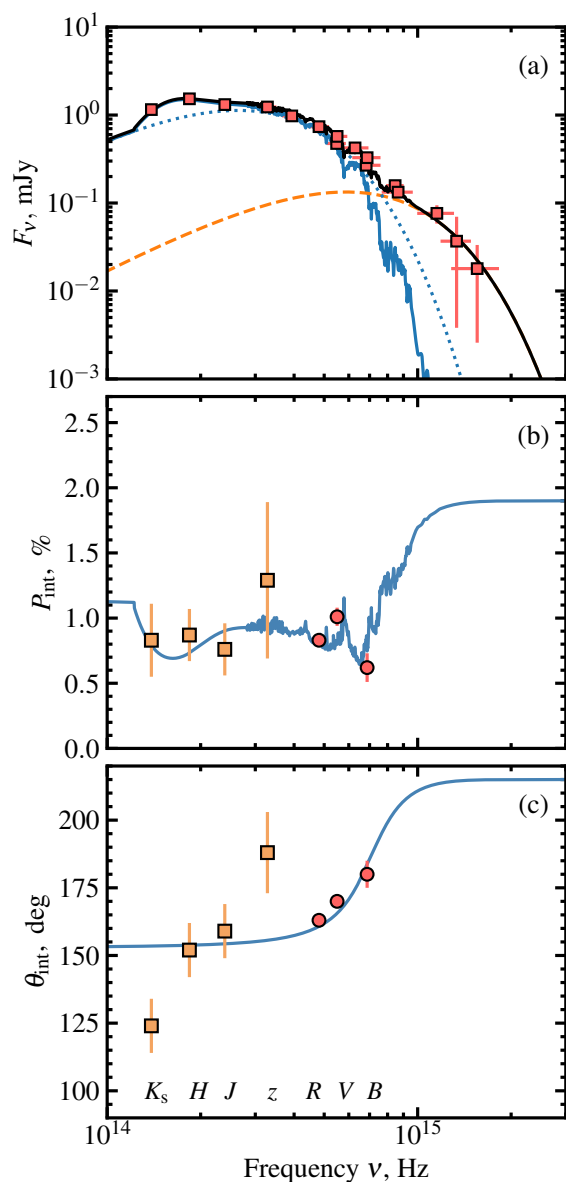


Fig. 9. Polarimetric properties of A0620–00. Panel (a): Energy dependence of flux F_ν as in Fig. 6 but only the data from this paper are shown. Panels (b) and (c): energy dependence of intrinsic PD and PA of A0620–00. Circles and squares correspond to optical observations from this paper and NIR polarimetric observations from Russell et al. (2016), respectively. Blue line corresponds to the model with two polarized components described in Sect. 4.1.

the scattered radiation, and spectrum as that of the optical companion (blue solid line in Fig. 9a). The additional UV component (dashed orange line), that was used to describe the UV part of the observed SED, is set to have constant PD and PA, whose values were free to vary. The blue lines in Fig. 9b,c show the dependence of PD and PA for this two-component scenario. The PD dependence on energy is noteworthy: P_V appears higher than P_B and P_R due to the narrow absorption of the stellar spectrum (and its scattering) in this band. We find the parameters $PA_{sc} \approx 150^\circ$, $PD_{sc} \approx 1\%$ for the stellar scattering and $PA_{UV} \approx 215^\circ$ with $PD_{UV} \approx 2\%$ for the UV component reproduce the energy dependence of PD and PA quite well (see Fig. 9b,c), especially in the optical band, where two components have comparable contribu-

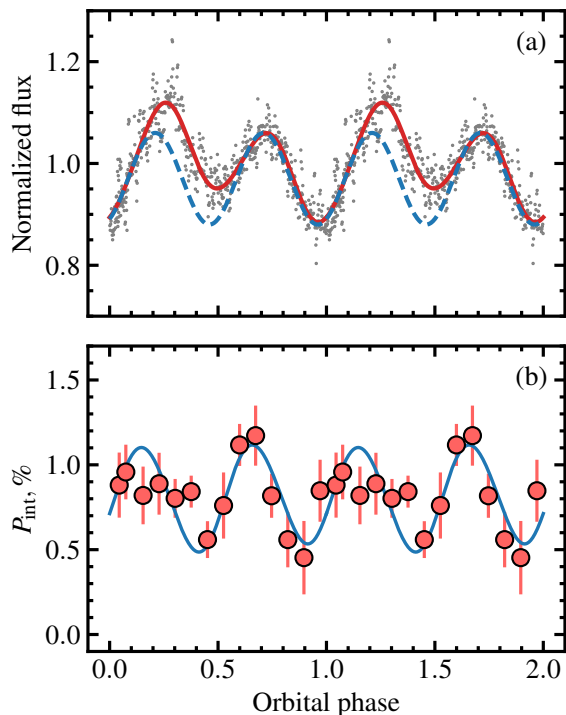


Fig. 10. Flux and PD variations of A0620–00. *Panel (a)*: the normalized flux, folded with the orbital phase (grey circles). Red solid line corresponds to the best fit of the data with the Fourier series, while the blue dashed line corresponds to the sinusoidal variations, assumed to be produced by the tidally distorted optical companion. *Panel (b)*: intrinsic PD of A0620–00 (red circles) folded with the orbital period together with the model of a scattering cloud on a circular orbit from the Appendix of Kravtsov et al. 2020 (blue line).

tion to the observed flux. The model is also generally consistent with the NIR points (taken decades earlier); some deviation in the K_s band might also arise from the Faraday effect or from the different treatment of the interstellar contribution to polarization.

The polarization of the UV component may arise from the first (single) Compton up-scattering of the disk or synchrotron photons by electrons in the hot accretion flow, similar to the case of MAXI J1820+070 (Poutanen et al. 2022). The difference of PA in the scattered and UV components can then indicate misalignment by $\sim 65^\circ$ (or $\sim 25^\circ$) between the axes of these components. This scenario predicts rise of PD and further rotation of PA towards the UV band (see Fig. 9). It can be tested in the future, by measuring polarization of A0620–00 simultaneously from NIR up to UV.

4.2. The source of the polarization variations

In addition to the changes in the polarization between different spectral states, we also see the orbital variations of the polarization. Although the 2% orbital modulation of the polarization observed by Dolan & Tapia (1989) has not been confirmed (Dubus et al. 2008), we see the variations at the level of 0.3% at the timescales of hours (see Fig. 5). To confidently claim that the polarization of A0620–00 is variable with the orbital phase one needs to cover at least two consecutive orbital periods with the high-precision polarimetric observations (which is a rather difficult task given the brightness of the object in quiescence and its short orbital period), we can still cautiously state that the

observed polarization variability is related to the orbital phase rather than having a stochastic nature. Indeed, the polarization of A0620–00, folded with the orbital phase shows the pattern, typical for binary stars – double-sinusoidal variations with the PD reaching minima in the conjunctions (phases 0 and 0.5) and maxima in the quadratures (phases 0.25 and 0.75), arising from Thomson scattering of the stellar radiation on the matter, following the compact object in its orbital motion (Brown et al. 1978; Kravtsov et al. 2020), and similar to these observed in another BH X-ray binary Cyg X-1 (Kemp et al. 1979; Kravtsov et al. 2023b). In Fig. 10, we see fairly good agreement of the PD variations with the expected behavior (blue line shows the model of a scattering cloud on a circular orbit, see Appendix of Kravtsov et al. 2020). In addition, our first and second observations, performed during two different orbits are consistent with each other (see Fig. 5).

The optical light curve shown in Fig. 10 has an asymmetric profile – the peak and the dip at the first half of the orbit are brighter than the other peak and dip. The so-called ellipsoidal variations of the flux, produced by the tidally distorted optical star (shown in blue dashed line at Fig. 10) cannot produce such asymmetry, therefore an additional source of flux variations is needed. There are two alternatives: either there is an additional bright component visible only at the first part of the orbit and generating additional flux (e.g. phase-dependent disk/bright spot, see e.g. Haswell et al. 1993), or some object blocks the light of the optical companion, reducing the total flux at phases from 0.5 to 1.0 (e.g. dark spots at the surface of the star, e.g. Cherepashchuk et al. 2019). We see similar asymmetry in the orbital polarization profile of A0620–00 – while around orbital phases from 0.5 to 1.0 the PD shows good agreement with the Thomson scattering model, at the first part of the orbit the PD is consistent with being constant. The additional bright unpolarized component, visible only at phases from 0.0 to 0.5 could reduce the polarization at these phases and explain both the asymmetric PD and flux variations, therefore we argue that the bright spot/phase-dependent disk model is more likely than the dark star spot model. Another alternative is that the asymmetric PD profile is produced by scattering of stellar radiation off slightly tilted accretion disk. In this scenario, the illuminated part of the accretion disk is visible to the observer only for half of the orbit (see Kravtsov et al. 2023b). However, scattering alone is not enough to reproduce $\sim 10\%$ increase of flux observed at the first half of the orbit, and the quality of our polarimetric data is not sufficient to discriminate between the complex models.

5. Conclusions

In this paper, we presented new high-precision phase-resolved optical polarimetric and quasi-simultaneous NIR-to-UV photometric observations of BH X-ray binary A0620–00 in a passive quiescent state. We determined and subtracted the interstellar polarization, which allowed us to derive the intrinsic polarization of A0620–00. Combined with the NIR polarimetric observations from Russell et al. (2016), we found that the orbit-average intrinsic PA rotates with the wavelength, changing from 124° in the K_s filter to 180° in B , while the PD remains at $\sim 1\%$ level throughout this spectral range. Folding our polarimetric observations with the orbital period, we found the significant orbital variability of polarization properties in the R band. The shape of the variations with two minima and two maxima per period suggest that the polarization is most probably produced by Thomson scattering of the companion star emission off the matter which follows the BH in its orbital motion (e.g. scattering off the ac-

cretion disk/stream). The lack of variations at the first part of the orbit suggests that either we see a depolarization effect caused by the bright spot visible only at these phases or (less probable) the scattering material producing the polarization is obscured or tilted relative to the orbital axis. However, more high-precision polarimetric observations during at least several consecutive orbital periods are needed to draw unambiguous conclusions about the geometry of the scattering medium.

The flat spectrum of the polarization and the presence of the orbital variations suggest that NIR-to-optical polarization has a scattering origin. However, in that case, the PA is not expected to change with the wavelength as observed. We first considered the possibility that stellar radiation scattered off the accretion disk experiences the Faraday rotation while traveling toward the observer through the magnetized plasma surrounding the accretion disk. The estimated values of magnetic field and optical depth can be consistent with realistic estimates if we consider our optical points in combination with the NIR points taken almost ten years ago. On the other hand, the steep trend of our optical points favour higher Faraday rotation rate, resulting in higher values for the line-of sight magnetic field.

We considered the scenario of two polarized components having different PDs and PAs. One component is coming from the stellar scattered light and the other associated with the additional UV component seen in the spectrum. The second component may potentially arise from Compton up-scattering of the disk or synchrotron photons in the hot inner flow, similar to that in the quiescent-state low-mass X-ray binary MAXI J1820+070. The PAs of these components differ by $\sim 65^\circ$, which translates to either 65° or 25° misalignment between their axes of symmetry. Future simultaneous polarimetric observations covering NIR-to-UV range would be extremely helpful in making an unambiguous choice between the models.

Acknowledgements. Based on observations made with the Nordic Optical Telescope, owned in collaboration by the University of Turku and Aarhus University, and operated jointly by Aarhus University, the University of Turku, and the University of Oslo, representing Denmark, Finland, and Norway, the University of Iceland and Stockholm University at the Observatorio del Roque de los Muchachos, La Palma, Spain, of the Instituto de Astrofísica de Canarias. The DIPol-2 and DIPol-UF polarimeters were built in cooperation between the University of Turku, Finland, and the Leibniz-Institut für Sonnenphysik, Germany. The Liverpool Telescope is operated on the island of La Palma by Liverpool John Moores University in the Spanish Observatorio del Roque de los Muchachos of the Instituto de Astrofísica de Canarias with financial support from the UK Science and Technology Facilities Council. MAPT acknowledge support from the Agencia Estatal de Investigación (MCIN/AEI) and the European Regional Development Fund under grant PID2021-124879NB-I00. This research has been supported by the Finnish Cultural Foundation (VK) and by the Academy of Finland grants 355672 (AV). Nordita is supported in part by NordForsk.

References

Arnaud, K. A. 1996, in ASP Conf. Ser., Vol. 101, *Astronomical Data Analysis Software and Systems V*, ed. G. H. Jacoby & J. Barnes (San Francisco: Astron. Soc. Pac.), 17

Brown, J. C., McLean, I. S., & Emslie, A. G. 1978, *A&A*, 68, 415

Cantrell, A. G., Bailyn, C. D., McClintock, J. E., & Orosz, J. A. 2008, *ApJ*, 673, L159

Cantrell, A. G., Bailyn, C. D., Orosz, J. A., et al. 2010, *ApJ*, 710, 1127

Cherepashchuk, A. M., Katysheva, N. A., Khruzina, T. S., et al. 2019, *MNRAS*, 483, 1067

Dinçer, T., Bailyn, C. D., Miller-Jones, J. C. A., Buxton, M., & MacDonald, R. K. D. 2018, *ApJ*, 852, 4

Dolan, J. F. 1976, *ApJ*, 210, 721

Dolan, J. F., & Tapia, S. 1989, *PASP*, 101, 1135

Dubus, G., Kern, B. D., Chaty, S., & Foellmi, C. 2008, in *Proceedings of Science*, Vol. 62, VII Microquasar Workshop: Microquasars and Beyond, 115

Elvis, M., Page, C. G., Pounds, K. A., Ricketts, M. J., & Turner, M. J. L. 1975, *Nature*, 257, 656

Froning, C. S., & Robinson, E. L. 2001, *AJ*, 121, 2212

Froning, C. S., Cantrell, A. G., Maccarone, T. J., et al. 2011, *ApJ*, 743, 26

Gaia Collaboration, Brown, A. G. A., Vallenari, A., et al. 2021, *A&A*, 649, A1

Gallo, E., Teague, R., Plotkin, R. M., et al. 2019, *MNRAS*, 488, 191

Garzón, F., Balcells, M., Gallego, J., et al. 2022, *A&A*, 667, A107

Gehrels, N., Chincarini, G., Giommi, P., et al. 2004, *ApJ*, 611, 1005

Gelino, D. M., Harrison, T. E., & Orosz, J. A. 2001, *AJ*, 122, 2668

Harrison, T. E., Howell, S. B., Szkody, P., & Cordova, F. A. 2007, *AJ*, 133, 162

Haswell, C. A., Robinson, E. L., Horne, K., Stiening, R. F., & Abbott, T. M. C. 1993, *ApJ*, 411, 802

Kemp, J. C., Barbour, M. S., Parker, T. E., & Herman, L. C. 1979, *ApJ*, 228, L23

Kosenkov, I. A., Berdyugin, A. V., Piirola, V., et al. 2017, *MNRAS*, 468, 4362

Kosenkov, I. A., Veledina, A., Berdyugin, A. V., et al. 2020, *MNRAS*, 496, L96

Kravtsov, V., Berdyugin, A., Veledina, A., et al. 2019, *The Astronomer's Telegram*, 13291, 1

Kravtsov, V., Nitindala, A. P., Veledina, A., et al. 2023a, *The Astronomer's Telegram*, 16245, 1

Kravtsov, V., Berdyugin, A. V., Piirola, V., et al. 2020, *A&A*, 643, A170

Kravtsov, V., Berdyugin, A. V., Kosenkov, I. A., et al. 2022, *MNRAS*, 514, 2479

Kravtsov, V., Veledina, A., Berdyugin, A. V., et al. 2023b, *A&A*, 678, A58

Kuulkers, E., Fender, R. P., Spencer, R. E., Davis, R. J., & Morison, I. 1999, *MNRAS*, 306, 919

Marsh, T. R., Robinson, E. L., & Wood, J. H. 1994, *MNRAS*, 266, 137

McClintock, J. E., Horne, K., & Remillard, R. A. 1995, *ApJ*, 442, 358

McClintock, J. E., & Remillard, R. A. 1986, *ApJ*, 308, 110

—, 2000, *ApJ*, 531, 956

Neilsen, J., Steeghs, D., & Vrtilik, S. D. 2008, *MNRAS*, 384, 849

Pickles, A. J. 1998, *PASP*, 110, 863

Piirola, V., Berdyugin, A., & Berdyugina, S. 2014, in *Proc. SPIE*, Vol. 9147, *Ground-based and Airborne Instrumentation for Astronomy V*, ed. S. K. Ramsey, I. S. McLean, & H. Takami, 914781

Piirola, V., Kosenkov, I. A., Berdyugin, A. V., Berdyugina, S. V., & Poutanen, J. 2021, *AJ*, 161, 20

Piirola, V., Berdyugin, A., Frisch, P. C., et al. 2020, *A&A*, 635, A46

Poutanen, J., Veledina, A., Berdyugin, A. V., et al. 2022, *Science*, 375, 874

Russell, D. M., Shahbaz, T., Lewis, F., & Gallo, E. 2016, *MNRAS*, 463, 2680

Schultz, J., Hakala, P., & Huovelin, J. 2004, *Baltic Astronomy*, 13, 581

Serkowski, K. 1962, *Advances in Astronomy and Astrophysics*, 1, 289

Shahbaz, T., Hynes, R. I., Charles, P. A., et al. 2004, *MNRAS*, 354, 31

Shahbaz, T., Ringwald, F. A., Bunn, J. C., et al. 1994, *MNRAS*, 271, L10

Steele, I. A., Smith, R. J., Rees, P. C., et al. 2004, in *Proc. SPIE*, Vol. 5489, *Ground-based Telescopes*, ed. J. M. Oschmann Jr., 679

van Grunsven, T. F. J., Jonker, P. G., Verbunt, F. W. M., & Robinson, E. L. 2017, *MNRAS*, 472, 1907

Veledina, A., Berdyugin, A. V., Kosenkov, I. A., et al. 2019, *A&A*, 623, A75

Wallace, J., & Pe'er, A. 2021, *ApJ*, 916, 63

Wu, C. C., Panek, R. J., Holm, A. V., Schmitz, M., & Swank, J. H. 1983, *PASP*, 95, 391